

Fire-spalling evaluation of concrete repaired with polymer cement mortar by ring-restrained heating test

*Makiho Sukekawa¹⁾, Yusuke Sugino²⁾, Toru Tanibe³⁾, Mitsuo Ozawa⁴⁾

1), 4) Gunma University, Department of Environmental Engineering Science, Japan

2), 3) Researcher, Taiheiyo Materials Corporation

ABSTRACT

In this research, we conducted a ring-restraint heating test to evaluate the spalling properties of specimens representing concrete that was assumed to have been repaired with polymer cement mortar (PCM). The restraint ring is made of steel with an outer diameter, height, and thickness of 300, 100, and 8 mm, respectively. The RABT30 rapid heating curve was used for the heating tests. To evaluate the effect of PCM repair thickness on the fire spalling damage, fire tests were performed using four types of specimens: two specimens with different thicknesses repaired with PCM (repair thickness: 50 and 20 mm), normal concrete specimen, and PCM specimen. The results showed that the concrete specimen repaired with PCM had a larger spalling scale than the normal concrete specimen. In addition, the specimen with a thicker PCM repair had a larger spalling scale than the specimen with a thinner repair.

1. INTRODUCTION

Polymer cement mortar (PCM), a material in which organic polymer is combined with cement mortar, is widely used as a cross-section repair material for concrete. It has become an indispensable material for repairing and reinforcing concrete structures because of its superior adhesion to concrete, compactness, and workability. On the other hand, the PCM contains organic polymers, which accelerate PCM spalling when exposed to high temperatures (Architectural Institute of Japan 2017). However, at present, the studies on PCM spalling are limited. Accordingly, our research group analyzed the spalling of PCM using the ring-restraint heating test method standardized by the Japan Concrete Institute (JCI) for evaluating the fire spalling of concrete (Japan Concrete Institute 2018). The assessment was conducted by measuring the main factors causing PCM spalling—thermal stress and vapor pressure. Further, the ring-restraint heating test method was used to determine the effect of the amount of added polymer (Sugino 2019). However, heating tests were not performed on actual concrete members repaired with PCM.

In this study, a concrete member repaired with PCM was simulated using a ring-restraint specimen. A heating test was conducted to examine the integration of concrete

and PCM. The experiment includes two PCM-repaired specimens with different thicknesses (repair thickness: 50 and 20 mm). Moreover, for comparison, normal concrete specimen (NSC) and PCM specimen (PCM-S) were prepared and subjected to heating tests. The spalling characteristics resulting from the difference in repair thickness and specimen material (i.e., PCM-S and NSC-S) of the four types of specimens were compared. The heating test results of the PCM-S specimen in this study are reproduced data derived by previous studies (Sugino 2019).

2. EXPERIMENTAL OUTLINE

2.1 Ring-restraint specimen

The outline of the JCI standard ring-restraint specimens is summarized in Table 1 and presented in Fig. 1. These specimens were of four types: PCM specimens with repair thicknesses of 50 and 20 mm (PCM50 and PCM20, respectively), PCM specimen (PCM-S), and normal strength concrete specimen (NSC). To simulate the reinforced concrete members, steel bars were placed in the PCM50 and NSC specimens set at a distance of 30 mm away from the heating surface.

Table. 1 Outline of the ring-restraint specimen

Specimen	Repair thickness (mm)	Polymer	P/C (%)	Measurement location (mm)	Steel bar location (mm)
NSC	-	-	-	5,10,40,60	30
PCM-S	-	Acrylic powder resin	10	5,10,25,40	-
PCM50	50			5,10,40,60	30
PCM20	20			5,10,30,40	-

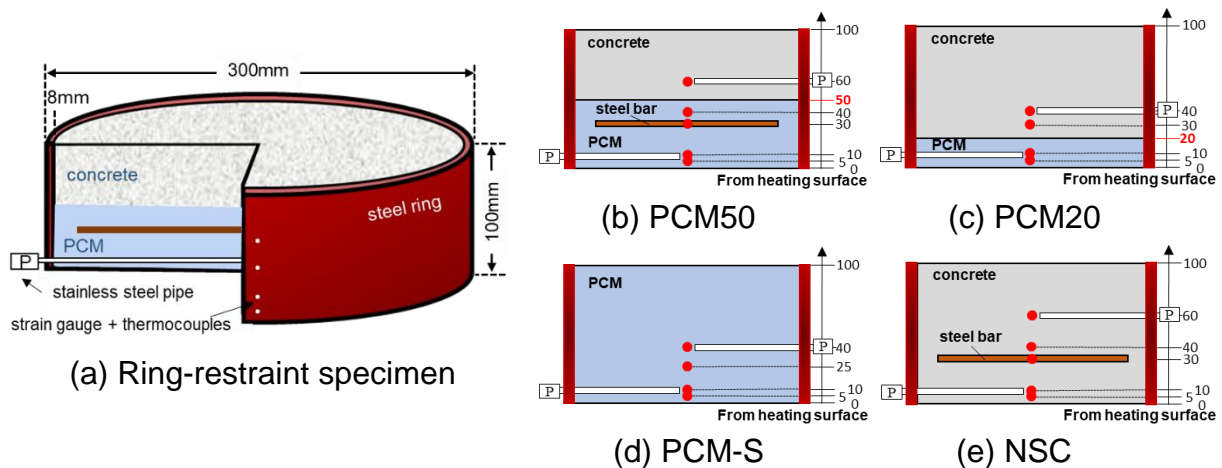


Fig. 1 Outline of the ring-restraint specimen

The testing ring is made of steel with an outer diameter, height, and thickness of 300, 100, and 8 mm, respectively. Four type-K thermocouples and four stainless steel pipes (outer diameter: 5 mm; inner diameter: 2 mm; length: 170 mm) were placed inside the specimens to measure the internal temperature and vapor pressure, respectively.

After filling the stainless-steel pipe with silicone oil, the pressure sensor was connected to determine the vapor pressure. Four strain gauges and four thermocouples were attached to the outer surface of the steel rings. The distances of the thermocouples, stainless steel pipes, and strain gauges from the heating surface were set as follows: 5, 10, 40, and 60 mm for PCM50 and NSC; 5, 10, 30, and 40 mm for PCM20; 5, 10, 25, and 40 mm for PCM-S.

After casting the concrete on the PCM50 and PCM20 specimens, the following treatment was applied to the joints. First, after the concrete had settled, the joint surface was sprayed with a treatment agent. Then, the concrete surface was washed using a brush to expose the coarse aggregates. Finally, the PCM was cast.

2.2 Concrete mixtures and fresh concrete properties

The concrete and PCM mixture proportions are summarized in Tables 2 and 3. The concrete water–cement ratio was 49.5 %, and ordinary Portland cement (density: 3.16 g/cm³) was used. Two types of fine aggregates, S1 and S2 (density: 2.64 and 2.61 g/cm³, respectively), and two types of coarse aggregates, G1 and G2 (density: 2.89 and 2.65 g/cm³, respectively), were used. The water–cement ratio of the PCM was 50 %, and the polymer cement mass ratio was 10 %; ordinary Portland cement was used. For the polymer, acrylic powder resin (density: 0.4–0.6 g/cm³) was used. The fine aggregate for the PCM was silica sand (density: 2.64 g/cm³).

The mechanical properties of fresh concrete and PCM are summarized in Tables 4 and 5, respectively. The concrete compressive strength was 43.1 MPa. The PCM-repaired specimens and PCM-S had the same PCM mix proportion, and their compressive strengths were 56.0 and 43.0 MPa, respectively; this difference in compressive strengths was influenced by the age of the material. The water contents of the PCM and concrete were 6.1 %–6.3 % and 5.7 %, respectively.

Table. 2 Concrete mixture proportion (NSC)

W/C (%)	Unit weight (kg/m ³)						Ad
	W	C	S1	S2	G1	G2	
49.5	183	370	439	439	634	271	4.07

Table. 3 PCM mixture proportion

P/C (%)	W/C (%)	NCM (kg/m ³)	Polymer (kg/m ³)	Water (kg/m ³)
10	50	197	5.63	28.2

Table. 4 Fresh properties

	Mixing temp. (°C)	PCM : Flow (mm) Concrete : Slump (cm)	Air (%)
PCM of repaired specimens	28.1	180	-
PCM-S	26.0	181	6.2
concrete	29.2	19.5	5.6

Table. 5 Mechanical properties

	compressive strength (MPa)	Tensile strength (MPa)	Elastic modulus (GPa)	Water content (mass%)
PCM of repaired specimens	56.0	3.9	22.4	6.3
PCM-S	43.0	2.8	22.0	6.1
concrete	43.1	2.8	30.3	5.7

2.3 Ring-restraint specimen heating test

The RABT30 rapid heating curve and gas furnace used in the heating test are shown in Figs. 2 and 3, respectively. The bottom of the ring-restraint specimen was heated, and insulation blankets were utilized to control the temperature rise in the ring. During the heating test, the age of PCM50, PCM20, and NSC was 3 months, and that of the PCM-S was 2 months. For safety, the heating test in the PCM-S was interrupted at approximately 15 min.

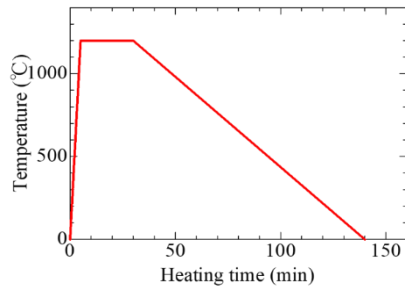


Fig. 2 RABT30 rapid heating curve



Fig. 3 Gas furnace

2.4. Restraint stress calculation

The restraint stress calculation was based on the strain measured in the steel ring in the circumferential direction, as given by Eq. (1).

$$\sigma_{re} = \varepsilon_{\theta} \cdot E_s \cdot t/R \quad (1)$$

where

σ_{re} : restraint stress in concrete or PCM (N/mm²);

ε_{θ} : circumferential direction strain in steel ring;

E_s : steel ring elastic modulus (N/mm²);

t : steel ring thickness (mm);

R : steel ring radius (mm).

2.5 Spalling scale evaluation (Japan Concrete Institute 2018)

The spalling scale was graded based on the condition of the bottom of the ring-restraint specimen after the heating test. The grading index of the spalling scale is summarized in Table 6. After spalling, the greatest depth of concrete or PCM loss in the measurement data was considered as the maximum spalling depth (D_{max}). Equations (2) and (3) show the calculation of the spalling area ratio (A_{sp}) and spalling floor space ratio (V_{sp}):

$$A_{sp} = N_i/N \quad (2)$$

$$V_{sp} = \sum D_i/(N \times H) \quad (3)$$

where

N_i : Explosive spalling area ratio rounded to nearest percent;

N : Number of measurement points;

$\sum D_i$: Total loss depth (mm);

H : Specimen height (mm).

Table. 6 Grading index of the spalling scale

Grade	Index 1	Index 2	Index 3
	Maximum spalling depth (D_{max})	Spalling area ratio (A_{sp})	Spalling floor space ratio (V_{sp})
A	No spalling, no microcracks.	No spalling, no microcracks.	No spalling, no microcracks.
B	No spalling, however microcracks existence.	No spalling, however microcracks existence.	No spalling, however microcracks existence.
C	Less than 10 mm.	Less than 10 %.	Less than 10 %.
D	10 to 30 mm.	10 to 50 %.	10 to 20 %.
E	More than 30 mm.	More than 50 %.	More than 20 %.

3. RESULT AND DISCUSSION

3.1 Heating surface damage and spalling scale evaluation

The results of the heating surface and spalling depth contours are shown in Fig. 4. The maximum spalling depths of PCM50 and PCM20 were 57 and 42 mm, respectively. The specimen with a thicker repair tended to have a larger spalling scale than that with thinner repair. In both specimens, the spalling reached the concrete part (assumed as the base material). The results indicate that the research on the use of a general method to prevent spalling must be continued. The maximum spalling depths of PCM-S (Sugino 2019) and NSC were 56 and 19 mm, respectively. Among the specimens, the spalling depth of NSC was the smallest. Although spalling occurred in PCM50 and PCM20, it halted near the interface between the PCM and base concrete, confirming that the PCM and concrete behaved as a unit during heating.

The temporal changes in the spalling depth of each specimen are shown in Fig. 5. In PCM50, PCM20, and PCM-S, spalling began approximately 5 min after heating started, reached the 40-mm depth at approximately 11–12 min, and then continued until 12–13 min. In the NSC, spalling occurred and stopped at 5 and 6 min after heating started, respectively.

The evaluation results of the spalling scale grading are summarized in Table 7. Specimens PCM50, PCM20, and PCM-S were all E grade with indices 1, 2, and 3, respectively. For the NSC, indices 1, 2, and 3 were 19 mm (D grade), 87 % (E grade), and 7 % (C grade), respectively. Thus, the spalling scale of the three specimens with PCM was larger than that of the NSC specimen. This indicates that during a fire event, there is an increased risk for the repaired RC members to spall.

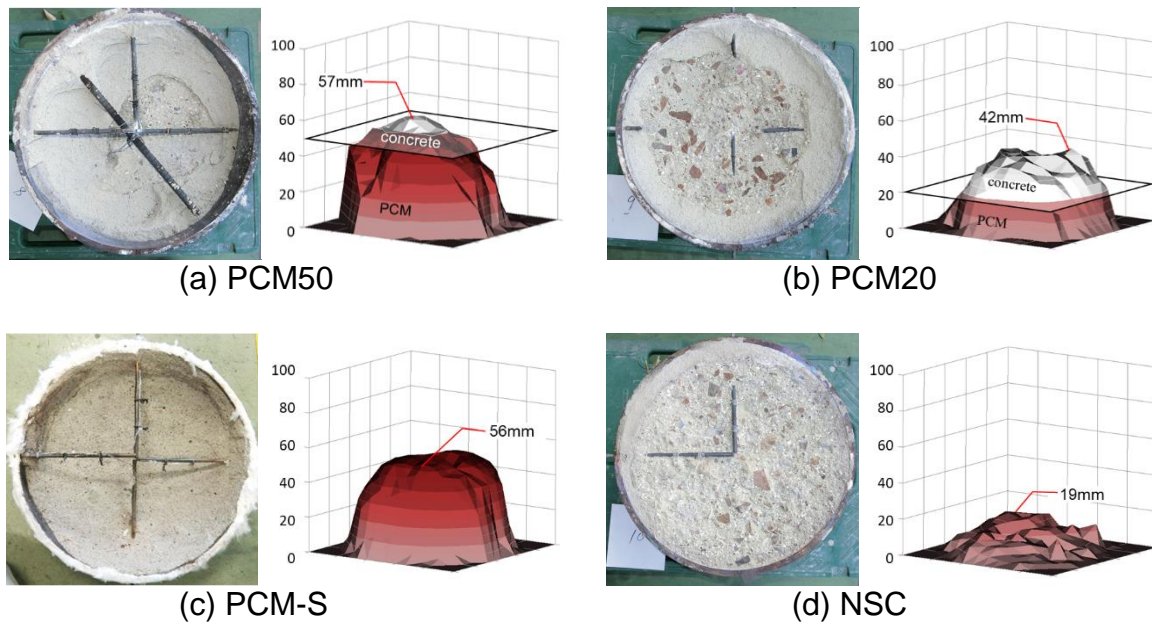


Fig. 4 Results of the heating surface and spalling depth contours

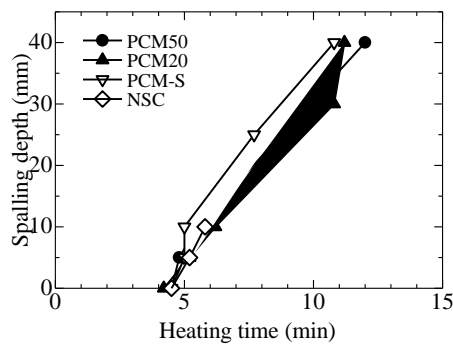


Fig. 5 Temporal changes in the spalling depth

Table. 7 The results of evaluation for spalling scale grading

	Situation of spalling			Grade		
	D_{max} (mm)	A_{sp} (%)	V_{sp} (%)	Index 1	Index 2	Index 3
PCM50	57	91	33	E	E	E
PCM20	42	92	22	E	E	E
PCM-S	56	98	36	E	E	E
NSC	19	87	7	D	E	C

3.2 Temporal changes in internal temperature

The temporal changes in the internal temperature at each measurement position from the heating surface of each specimen are shown in Fig. 6. It was confirmed that the internal temperature of PCM50 increased rapidly at distances of 5, 10, and 40 mm from the heating surface (Fig. 6(a)) as a result of the thermocouple exposure to the furnace because of spalling. A similar rapid temperature rise was also observed at the position

where spalling occurred in PCM20, PCM-S, and NSC (Fig. 6, (b)–(d), respectively). Although spalling occurred in PCM50 and NSC, the surface temperatures of the steel bars of PCM50 and NSC remained at 120 and 60 °C (Fig. 6, (a) and (d)), respectively. It is apparent that the surface temperatures of steel bars could not be measured accurately.

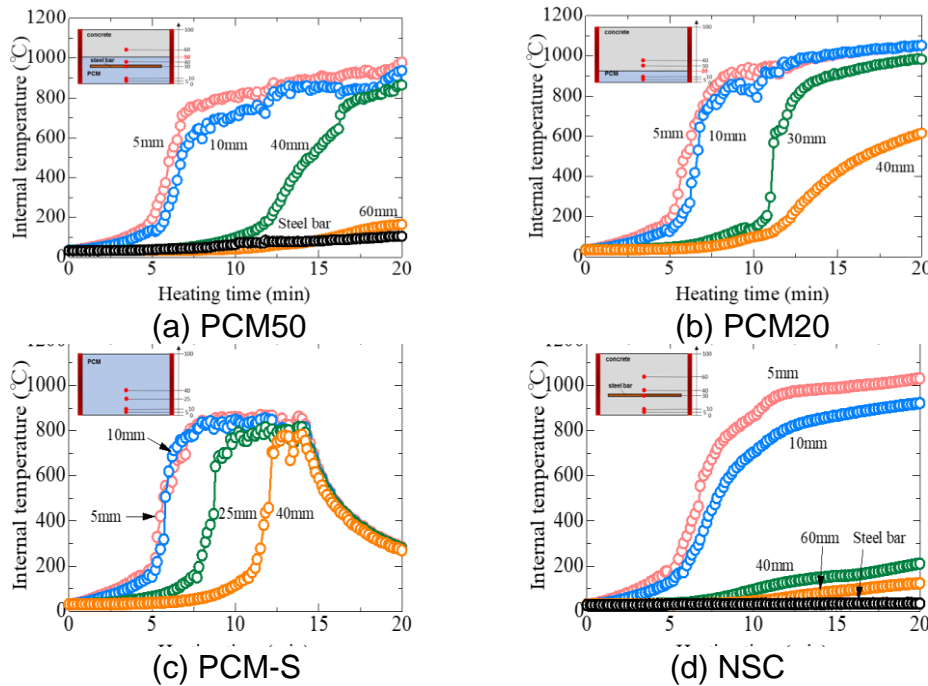
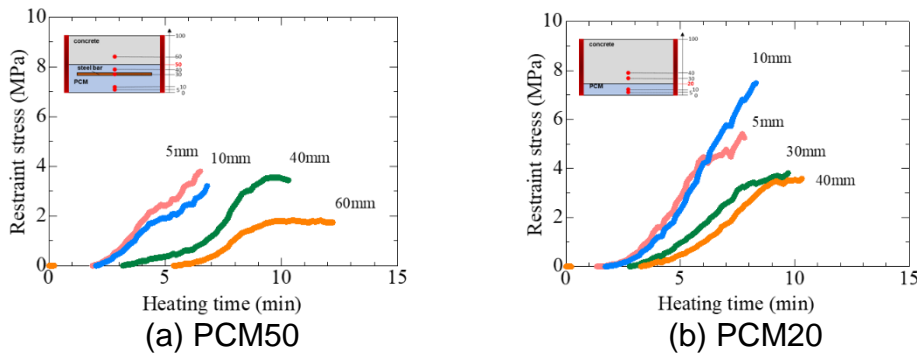
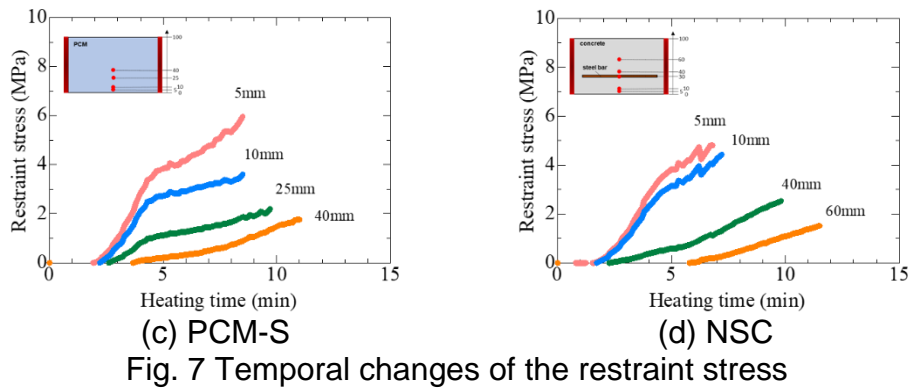


Fig. 6 Temporal changes of the internal temperature

3.3 Temporal changes in restraint stress

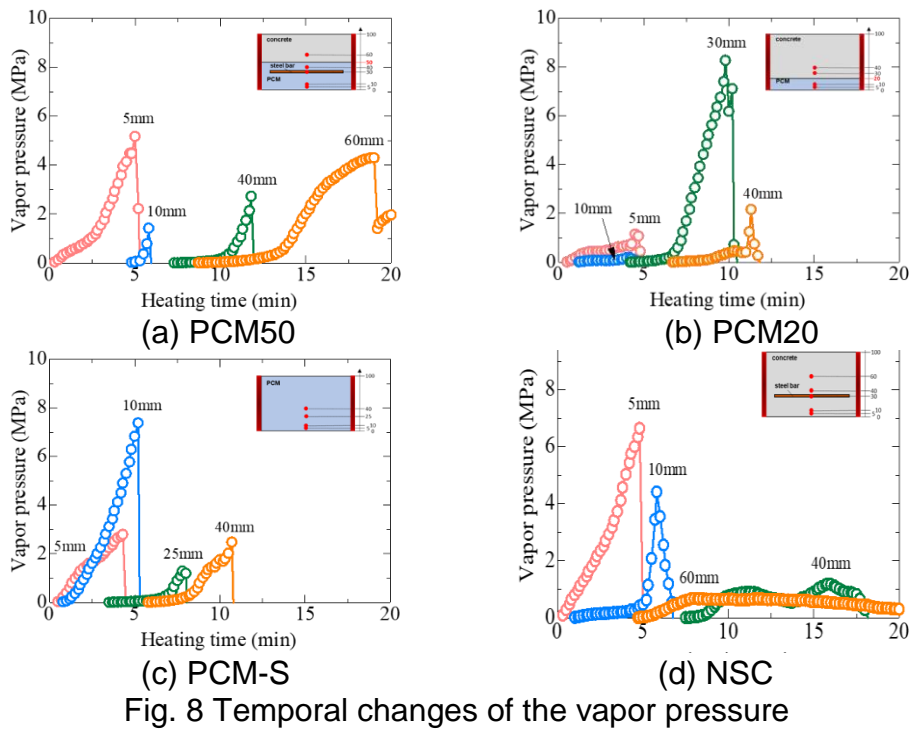
The temporal changes in the restraint stress in each specimen are shown in Fig. 7. The PCM50 restraint stress at the 5-mm distance from the heating surface was relieved after 4 min of heating because of the thermal decomposition of cement hydration products and microcracks induced by heating (Fig. 7(a)). Thereafter, the restraint stress increased and then rapidly decreased because of spalling. This behavior is also observed in PCM20, PCM-S, and NSC at 5 and 10-mm distances from the heating surface (Fig. 7, (b)–(d), respectively). The maximum restraint stress values for PCM50, PCM20, PCM-S, and NSC were 3.8, 7.5, 6.0, and 4.8 MPa, respectively.





3.4 Temporal changes in vapor pressure

The temporal changes in the vapor pressure in each specimen are shown in Fig. 8. The vapor pressure rapidly increased and then sharply decreased because of the spalling in the specimens. No sharp decrease in vapor pressure was observed at the measurement positions where no spalling occurred (Fig. 8(d)). The vapor pressure values at the 60 and 30-mm positions in PCM50 and PCM20 significantly increased (Fig. 8, (a) and (b), respectively). This phenomenon was attributed to the influence of accumulated moisture at the interface between the PCM and concrete. Previous studies reported that during heating, the moisture in a specimen moved upward from the heating surface (Jansson 2013). Other studies reported that the moisture in concrete can easily move up to the interface between the concrete and repair material under normal temperatures (Ueda 2010). In this case, it is presumed that the permeability of concrete and PCM has a certain influence; however, further research is necessary to verify this.



3.5 Assumptions in spalling mechanism of concrete and PCM

In previous studies, the spalling mechanism was explained by the thermal dilation theory (Bazant 1997), vapor pressure theory (Anderberg 1997), and their combination. In this research, the following are assumed in the spalling mechanism of concrete.

- ① The restraint stress acts in a direction parallel to the heating surface because of heating.
- ② The tensile strain acts in a direction vertical to the heating surface because of the Poisson effect. After the tensile strain exceeds the limit value, horizontal microcracks occur in the fine voids and matrix inside the concrete (Tanibe 2011).
- ③ The moisture in the fine voids of concrete transforms into vapor during heating and exerts vapor pressure thereafter.
- ④ Due to ② and ③, the vapor pressure acts on the microcracks; the fracture surface expands, causing spalling.

Based on the foregoing assumptions, the spalling mechanism is discussed as follows.

3.6 Internal temperature, restraint stress, and vapor pressure

The relationship between the internal temperature, restraint stress, and vapor pressure at a 5-mm distance from the heating surface are shown in Fig. 9; the figure also shows the saturated vapor pressure (SVP) curve and internal temperature at the time of spalling. Ichikawa et al. (Ichikawa 2004) reported the relationship between the internal temperature and vapor pressure in concrete (SVP graph: left, saturated zone; right, dry zone).

In PCM50 (Fig. 9(a)), the restraint stress started to increase at 130 °C; beyond 130 °C, the restraint stress was approximately 2 MPa. At 150 °C, spalling occurred at a distance of 5 mm from the heating surface and the vapor pressure increased to 4 MPa. On the other hand, at 180 °C, the restraint stress in PCM20 started to increase; it was approximately 3 MPa beyond 180 °C. The vapor pressure continued to be less than 1 MPa, and spalling occurred when the distance from the heating surface was 5 mm and the temperature was approximately 200 °C. The spalling mechanism is considered to be similar to the assumptions above. However, the low vapor pressure in PCM20 was caused by the movement of moisture into the interface between the concrete and PCM. As shown in Fig. 8(b), the vapor pressure is low and high at the 10-mm and 30-mm locations (before and beyond the interface), respectively.

In the NSC (Fig. 9(b)), it can be observed that the restraint stress and vapor pressure continued to increase up to a temperature of 150 °C, with the restraint stress reaching 4 MPa. Thereafter, with a 5-mm distance from the heating surface, spalling occurred, and the vapor pressure sharply decreased. This was caused by the increase in the restraint stress and vapor pressure induced by heating and the occurrence of microcracks. After the microcracks occurred, the restraint stress did not increase. Thereafter, spalling occurred because of the vapor pressure acting on the microcracks. In contrast, the restraint stress and vapor pressure in PCM-S were similar to those of the NSC. Therefore, the spalling mechanism of the PCM-S is similar to the assumptions above. However, the maximum vapor pressures in PCM-S and NSC differed, i.e., 6.6

and 2.8 MPa, respectively. This difference is presumed to be related to permeability; however, further research is necessary to confirm this.

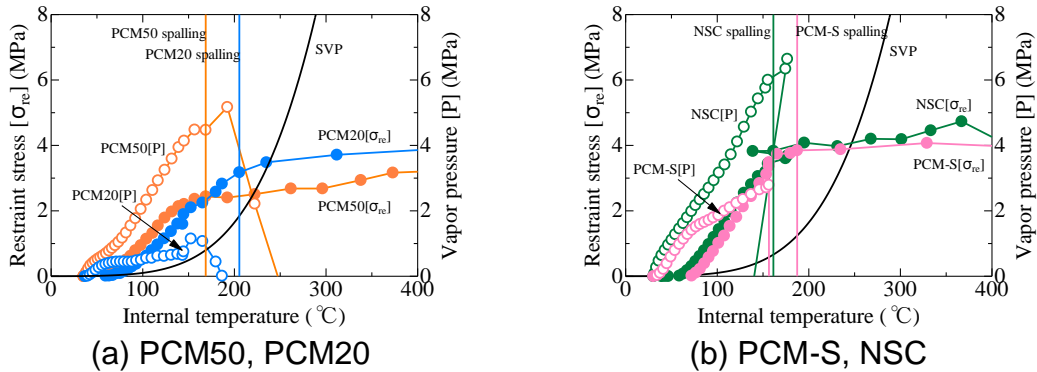


Fig. 9 Internal temperature, restraint stress, and vapor pressure at 5 mm

The relationship between internal temperature, restraint stress, and vapor pressure at a 40-mm distance from the heating surface is shown in Fig. 10. At a temperature of 80 °C, the restraint stress in PCM50 and PCM20 was constant at approximately 3.5 MPa. The maximum vapor spalling pressures in PCM50 and PCM20 were 2.7 and 2.2 MPa, respectively.

In the NSC (Fig. 10(b)), the maximum spalling depth was 19 mm; hence, no spalling occurred at the measurement location of 40 mm from the heating surface, and no sharp decrease in the vapor pressure was observed. It is also presumed that the low water vapor pressure is caused by the easy escape of pressure through the thermal decomposition of hydration products in the concrete and fine cracks. It can be observed that it was difficult for the restraint stress in the PCM-S to increase when the distance from the heating surface was at 40 mm than at 5 mm. This is presumed to be related to the heat damage and formation of spalling surfaces.

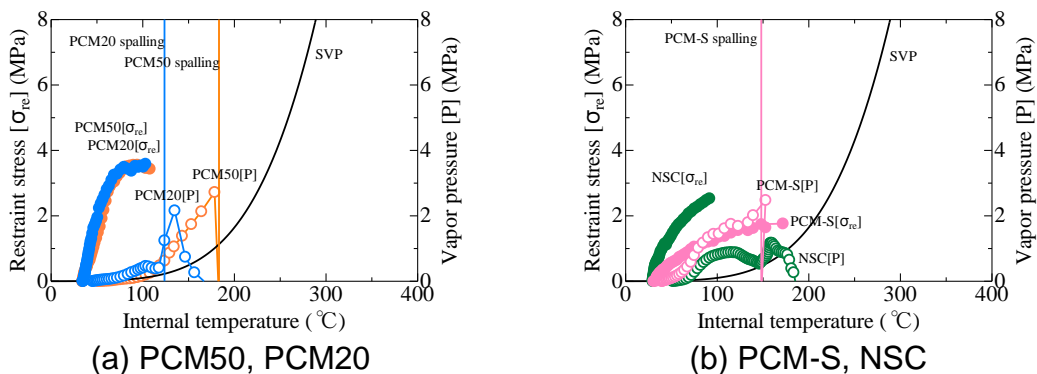
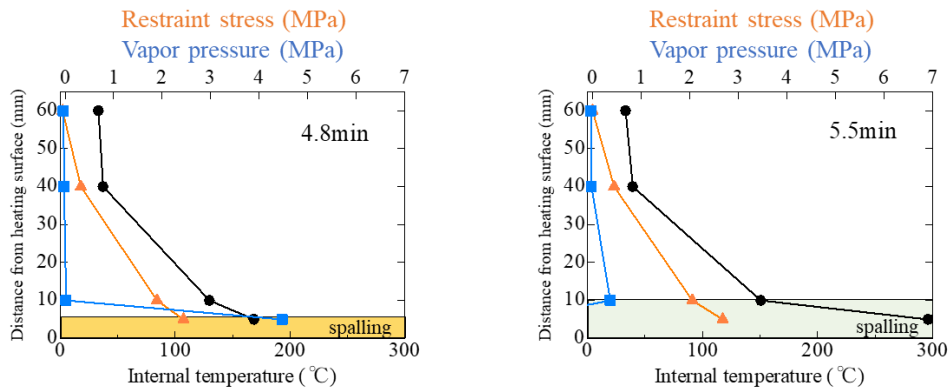


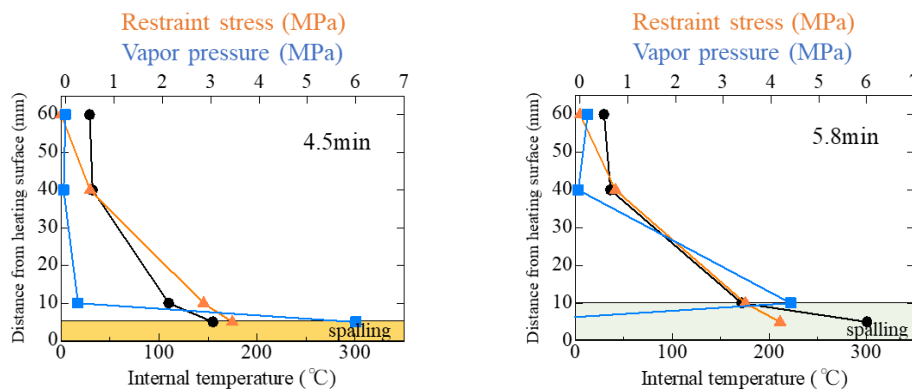
Fig. 10 Internal temperature, restraint stress, and vapor pressure at 40 mm

The relationship between the internal temperature, restraint stress, and vapor pressure at each measurement location when spalling occurs in PCM50 and NSC is shown in Fig. 11. It is observed that the restraint stress and internal temperature are higher at positions near the heating surface. In the case of PCM50 and NSC, gradients in internal temperature, restraint stress, and vapor pressure were observed. The restraint

stress and vapor pressure at 4.8 min were 2.5 and 4.5 MPa, respectively; the vapor pressure was highest at the spalling depth point. Thereafter, when spalling occurred at 5.5 and 5.8 min, the vapor pressure gradually increased at the 10-mm position because the moisture in the specimen moved in the depth direction induced by heating.



(a) PCM50 at 4.8 and 5.5 min



(b) NSC at 4.5 and 5.8 min

● Internal temperature ▲ Restraint stress ■ Vapor pressure

Fig. 11 Each measurement location when spalling occurs in PCM50 and NSC

4. CONCLUSIONS

The results of this study are summarized as follows.

- 1) With the assumption that the concrete was repaired with the PCM, the result of the ring-restraint heating test indicated that the spalling of specimens reached the concrete part, which is assumed as the base material. It was deduced from this study that an actual member repaired with the PCM will be confronted with the risk of spalling. Accordingly, it is necessary to extend this research using a general approach to preclude spalling.
- 2) The specimen with a thicker repair material tended to have larger spalling scale than that with thinner repairs.

*The 2020 World Congress on
The 2020 Structures Congress (Structures20)
25-28, August, 2020, GECE, Seoul, Korea*

- 3) It is possible to evaluate the spalling properties in a specimen by assuming it as a repaired member and using the relationship between restraint stress, vapor pressure, and internal temperature obtained by the ring-restraint heating test method.

ACKNOWLEDGMENT

This study was financially supported by a Grant-in-Aid for Scientific Research (C) (General) from the Japan Society for the Promotion of Science (No.19K04546; Head: Dr. M. Ozawa) and the Obayashi Foundation. The authors would like to express their gratitude to these organizations for their financial support.

REFERENCES

- Architectural Institute of Japan (2017), "Guidebook for fire-resistive performance of structural materials." (In Japanese)
- Japan Concrete Institute (2018), "Test Method for Spalling of Concrete under High Temperature Exposure." JCI-S-014-2018.
- Sugino, Y., Tanibe, T., Roppongi, H., Ozawa, M. (2019), "Behavior of ring-restrained polymer-modified mortar using acrylic resin during the fire", Proceedings of the Japan Concrete Institute, Vol. 41(1), 1001–1006. (In Japanese)
- Jansson, R. (2013), "Fire spalling of concrete theoretical and experimental studies." Doctoral thesis in concrete structures, Stockholm, Sweden, 18.
- Ueda, H., Kudo, T., Tamai, Y. (2010), "Evaluation of durability on cement-based repair materials." RTRI Report, Vol. 24(8).
- Bazant, Z.P. (1997), "Analysis of pore pressure, thermal stress and fracture in rapidly heated concrete, in: L.T. Phan, N.J. Carino, D. Duthinh, E. Garboczi (Eds)", Proceedings of the international workshop on fire performance of high-strength concrete, Gaithersburg, Maryland, NIST, 155–164.
- Anderberg, Y. (1997), "Spalling phenomena in HPC and OC, in: L.T Phan, N.J. Carino, D. Duthinh, E. Garboczi (Eds.)", Proceedings of the international workshop on fire performance of high-strength concrete, Gaithersburg, Maryland, NIST, 69–73.
- Tanibe, T., Ozawa, M., Lustoza, D. R., Kikuchi, K., Morimoto, H. (2011), "Explosive spalling behavior of restrained concrete in the event of fire." 2nd International RILEM Workshop on Concrete Spalling due to Fire Exposure, Delft (Netherlands), 319–326.
- Ichikawa, Y., England, G. L. (2004), "Prediction of moisture migration and pore pressure build-up in concrete at high temperature." Nuclear Engineering and Design Vol. 228, 245–259.